

REPORT DOCUMENTATION PAGE

AFRL-SR-AR-TR-03-

Public reporting burden for this collection of information is estimated to average 1 hour per response, including gathering and maintaining the data needed, and completing and reviewing the collection of information. Send collection of information, including suggestions for reducing this burden, to Washington Headquarters Service, Davis Highway, Suite 1204, Arlington, VA 22202-4302, and to the Office of Management and Budget, Paper

ces,
this
son

0253

1. AGENCY USE ONLY (Leave blank)		2. REPORT DATE	3. REPORT NUMBER
			15 JUL 2000 - 31 MAY 2003 Final Report
4. TITLE AND SUBTITLE 94GHZ High-Average-Power Broadband Amplifier			5. FUNDING NUMBERS 61102F 2301/EX
6. AUTHOR(S) Dr McDermott			
7. PERFORMING ORGANIZATION NAME(S) AND ADDRESS(ES) UNIVERSITY OF CALIFORNIA 410 MRAK HALL DAVIS CA 95616-8671			8. PERFORMING ORGANIZATION REPORT NUMBER
9. SPONSORING/MONITORING AGENCY NAME(S) AND ADDRESS(ES) AFOSR/NE 4015 WILSON BLVD SUITE 713 ARLINGTON VA 22203			10. SPONSORING/MONITORING AGENCY REPORT NUMBER F49620-00-1-0339
11. SUPPLEMENTARY NOTES			
12a. DISTRIBUTION AVAILABILITY STATEMENT APPROVED FOR PUBLIC RELEASE, DISTRIBUTION UNLIMITED			
20030731 047			
13. ABSTRACT (Maximum 200 words) <p>A state-of-the-art gyro-TWT amplifier operating in the low loss TE01 mode has been developed with the objective of producing an average power of 140 kW in the W-Band with a predicted efficiency of 28%, 50dB gain, and 5% bandwidth. The primary objective is to increase the bandwidth of W-band gyrotron amplifiers to several percent by employing a stable high performance gyro-TWT circuit. The amplifier was developed for the extremely important electromagnetic W-Band for future DoD millimeter-wave applications, in particular for the WARLOC radar. Our innovative amplifier has further improved upon the characteristics of the recent NRL-industry high average power W-Band TE01 gyro-klystron and gyro-twstron amplifiers. The bandwidth has been increased by nearly an order of magnitude.</p> <p>The suppression of gyro-BWO oscillation was a critical factor in the design of the TErn gyro-TWT. However, it should be noted that this negative-feedback interaction can be very useful by itself. In particular, a dual mode gyro-BWO has been designed to yield high power in the W-Band over a broad bandwidth, which will provide vital capability for future ECM applications. The two tuning modes of our gyro-BWO are fast tuning by changing the cathode voltage and slow tuning by changing the magnetic field. It will utilize much of the TE01 gyroTWT circuit. The tapered device is predicted to generate 100 kW near 94 GHz with over 10% tuning and 20% efficiency.</p>			
14. SUBJECT TERMS infrared fiber optics, hollow glass waveguides, metal sulfide thin film, wet chemistry processing, Cadmium sulfide, Lead Sulfide			15. NUMBER OF PAGES
			16. PRICE CODE
17. SECURITY CLASSIFICATION OF REPORT UNCLASSIFIED	18. SECURITY CLASSIFICATION OF THIS PAGE UNCLASSIFIED	19. SECURITY CLASSIFICATION OF ABSTRACT UNCLASSIFIED	20. LIMITATION OF ABSTRACT UL

AFOSR Final Progress Report

7/15/2000 – 5/31/2003

94 GHz High-Average-Power Broadband Amplifier

AFOSR Grant F49620-00-1-0339

Principal Investigator: N.C. Luhmann, Jr.

Department of Applied Science

University of California, Davis

The Regents of the University of California

University of California, Davis

410 Mrak Hall

Davis, CA 95616

94 GHz High-Average-Power Broadband Amplifier
AFOSR Final Progress Report 7/15/2000 – 5/31/2003

Table of Contents

1.0	Research Objectives	3
2.0	Synopsis of Research Results and Program Status	4
3.0	Quad Chart of 94 GHz High-Average-Power Broadband Amplifier Program	5
4.0	Significant Accomplishments	6
5.0	Research Progress	7
5.1	Heavily Loaded TE₀₁ Gyro-TWT Amplifier	7
5.1.1	Design	7
5.1.2	Experimental Measurements	17
5.2	TE₀₁ Gyro-BWO	22
5.2.1	Design	22
5.2.2	Theory -- Start-Oscillation Current of Lossy Gyro-BWO	26
6.0	Personnel	31
7.0	Publications and Presentations	31
8.0	Patents	33
9.0	Honors	33

AFOSR Performance Report – 8/1/2001-7/31/2002

1.0 Research Objectives

A state-of-the-art gyro-TWT amplifier operating in the low loss TE_{01} mode has been developed with the objective of producing an average power of 140 kW in the W-Band with a predicted efficiency of 28%, 50 dB gain, and 5% bandwidth. The primary objective is to increase the bandwidth of W-band gyrotron amplifiers to several percent by employing a stable high performance gyro-TWT circuit. The amplifier was developed for the extremely important electromagnetic W-Band for future DoD millimeter-wave applications, in particular for the WARLOC radar. Our innovative amplifier has further improved upon the characteristics of the recent NRL-industry high average power W-Band TE_{01} gyro-klystron and gyro-twstron amplifiers. The bandwidth has been increased by nearly an order of magnitude.

The suppression of gyro-BWO oscillation was a critical factor in the design of the TE_{01} gyro-TWT. However, it should be noted that this negative-feedback interaction can be very useful by itself. In particular, a dual mode gyro-BWO has been designed to yield high power in the W-Band over a broad bandwidth, which will provide vital capability for future ECM applications. The two tuning modes of our gyro-BWO are fast tuning by changing the cathode voltage and slow tuning by changing the magnetic field. It will utilize much of the TE_{01} gyro-TWT circuit. The tapered device is predicted to generate 100 kW near 94 GHz with over 10% tuning and 20% efficiency.

2.0 Synopsis of Research Results and Program Status

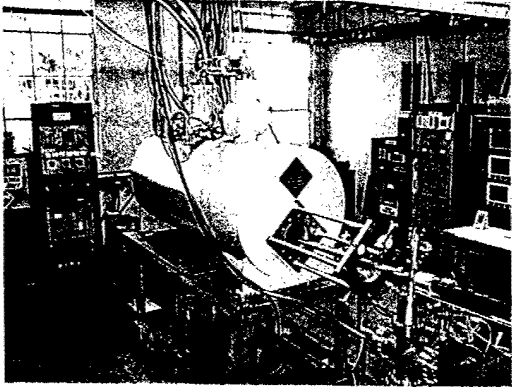
This program was launched with Dr. David McDermott as the Principal Investigator with close coordination and cooperative activities with the MURI99 Innovative Vacuum Electronics Initiative. Unfortunately, due to deteriorating health Dr. McDermott was forced to retire on medical disability resulting in the Investigatorship passing to N.C. Luhmann, Jr. for the final phases. However, it is stressed that the overall experiment design was due to Dr. McDermott and that he remains actively involved within the limits dictated by his physical condition.

The UCD single-stage heavily loaded W-Band gyro-TWT has been tested at full RF input power using a 100 W folded waveguide TWT driver with a bandwidth of 5%. Preliminary measurements, made at lower voltage than the design value of 100kV, yielded 53kW saturated power with 47dB gain, 14% efficiency, and 1.1% bandwidth. Efforts are continuing to further optimize the device and are expected to yield performance closer to the design values. In addition a broader band input coupler has been fabricated and tested to increase the amplifier's bandwidth to 5%.

Our paper, "Design of a High Power W-Band Heavily Loaded TE₀₁ Gyro-TWT Broadband Amplifier," which describes the stabilization procedure and design of this high energy density amplifier, has been published in the IEEE Transactions on Plasma Science's most recent Special Issue on High Power Microwave Generation (June 2002). Of related interest, researchers at NRL, who have copied this design procedure to construct a 35 GHz amplifier with a different loss structure, have also published a paper in the Special Issue that also shows that the device is stable and efficient.

We have also obtained W-Band power levels on the order of 100 kW by detuning the device into a gyro-BWO. The experimental start oscillation current agrees qualitatively with our theoretical derivation. In addition, a separate, specially designed, tapered TE₀₁ gyro-BWO has been fabricated which is predicted to generate 100 kW near 94 GHz with over 10% tuning and 20% efficiency. The gyro-BWO has been modeled with a self-consistent particle-tracing simulation code and will be tested after the gyro-TWT.

3.0 Quad Chart of 94 GHz High-Average-Power Broadband Amplifier Program

<p>Objectives</p> <ul style="list-style-type: none">• Extend DoD's broadband amplifier technology into the millimeter range• Develop stable W-band	<p><i>50 kW Superconducting</i></p> 
<p>Approach</p> <ul style="list-style-type: none">• Gyro-TWT's offer wide bandwidth• TE₀₁ mode transmits high power	<p>Accomplishments</p> <ul style="list-style-type: none">• High power W-Band gyro-TWT is under operation and is stable• 53 kW generated with 47 dB gain, 1.1 % bandwidth and 14% efficiency in initial hot tests• Large-signal code predicts 28% efficiency• $\cong 100$ kW generated when detuned as gyro-BWO

4.0 Significant Accomplishments

- The UCD heavily loaded W-Band TE_{01} gyro-TWT is stable and has yielded an output power of 53 kW with 14% efficiency, 47 dB large-signal gain, and a bandwidth of 1.1% in initial hot tests.
- A new input coupler with a bandwidth of 10% has been fabricated to increase the amplifier's bandwidth to the full design value of 5%.
- A new MIG electron gun with angled electrodes was fabricated and utilized after being designed with EGUN with a predicted axial velocity spread of 2.2 %.
- A 25 kV modulator was constructed in collaboration with our MURI colleagues at SLAC to power either of our kilowatt level W-Band pulsed RF sources with 5% tuning--a 1 kW EIO and a 100 W TWT amplifier--in order to drive the test the gyro-TWT amplifier at saturation.
- Power levels of $\cong 100$ kW have been produced by detuning the gyro-TWT into a gyro-BWO.
- A theory of the gyro-BWO in a lossy circuit was developed.
- The measured value of the gyro-BWO start oscillation current is in relatively good agreement with the new theory.
- A separate gyro-BWO circuit has been designed to generate 150 kW at 94 GHz with 10% tuning and 20% efficiency by employing a self-consistent large-signal code.
- The tapered TE_{01} gyro-BWO circuit has been fabricated.
- Our paper that describes the stabilization procedure and design of the high power W-Band gyro-TWT amplifier was published in the IEEE Transactions on Plasma Science's most recent Special Issue on High Power Microwave Generation (June 2002).
- UC Davis graduate students Heather Song, Hsin-Lu Hsu and Jase Lee, who have participated in the development of these devices, passed their PhD qualifying comprehensive exams.

5.0 Research Progress

5.1 Heavily Loaded TE_{01} Gyro-TWT Amplifier

5.1.1 Design

The amplifier design was developed by following the marginal stability design procedure. Because a large axial velocity is beneficial for stability and wide bandwidth, the operating voltage of a high power gyro-TWT should be as high as practical. Consequently, a voltage of 100 kV was chosen. To reduce the interception of electrons by the wall, the guiding center of the beam selected to be 45% of the wall radius, which is slightly inside of the mode maximum. Small-signal codes were employed to investigate the stability of the amplifier. First, the amplifier must remain stable from the absolute instability of the operating mode, which occurs when the gain is sufficiently high that the bandwidth extends to the cutoff frequency. At this point, a wave at cutoff will become unstable and a backward wave will start to grow. The threshold electron beam current for this from saddle-point theory is shown in Fig. 1 for a 100 kV beam whose guiding center radius, r_c , is 45% of the wall radius. Since the TE_{01} mode is predicted to oscillate at 10 A for our design parameters (100 kV, $v_{\perp}/v_z = 1.0$, $B/B_g = 0.995$) in a lossless circuit and loss will add further stability, there was felt to be a comfortable safety margin for our beam current of 5 A.

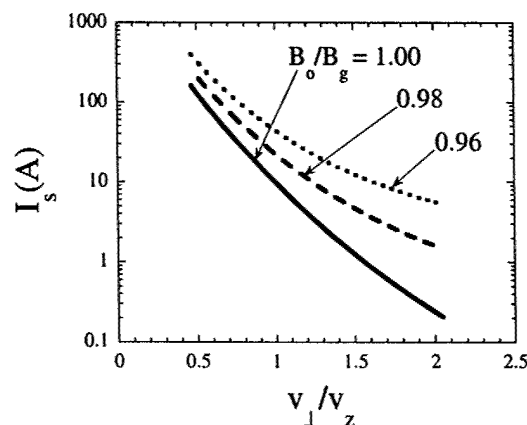


Fig. 1. Dependence of threshold current for absolute instability on velocity ratio $\alpha = v_{\perp}/v_z$ for three values of magnetic field (100 kV, $r_c/r_w = 0.45$).

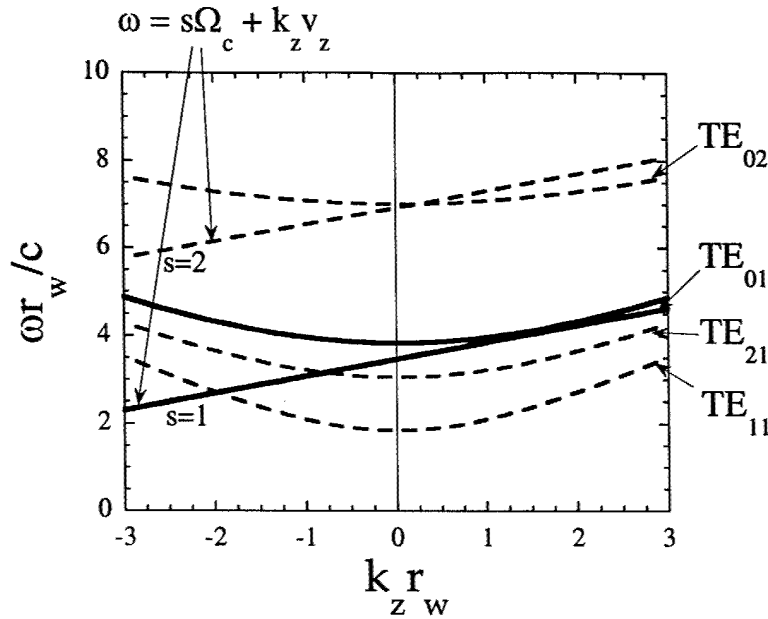


Fig. 2. Dispersion diagram of the operating mode (intersection of unbroken curves) and possible oscillating modes (intersections of broken curves with negative k_z) (100 kV, $v_{\perp}/v_z = 1.0$).

The dispersion diagram for the amplifier is shown in Fig. 2. To yield strong amplification over the broadest bandwidth, the cyclotron resonance line nearly grazes the TE_{01} mode. To enhance the efficiency, the magnetic field is slightly detuned ($B/B_g = 0.995$, where B_g is the grazing magnetic field). It is evident there are several potential gyro-BWO modes at the fundamental cyclotron frequency and at the harmonics. The short interaction length needed to stabilize these modes would yield insufficient gain to even overcome the launching loss. However, a recent gyro-TWT experiment at NTHU has found that loss can stabilize gyro-BWO modes. The critical length for the start of gyro-BWO oscillation in the amplifier with loss and an ideal beam is shown in Fig. 3. Generally, modes that are excited near their cutoff, where the wave impedance is highest, have the lowest start-oscillation length. However, wall loss is more effective close to the cutoff. The $TE_{02}^{(2)}$ mode (the superscript refers to the harmonic number) is closest to cutoff and seen to be most sensitive to wall loss. The $TE_{11}^{(1)}$ mode is least sensitive; however, it was anticipated that it will be stabilized by the beam's velocity spread. For a wall resistivity of $70,000\rho_{Cu}$, where ρ_{Cu} is the resistivity of ideal copper ($\rho_{Cu} = 1.72 \times 10^{-6} \Omega \text{ cm}$), the $TE_{21}^{(1)}$ mode is stable for an interaction length of 15 cm.

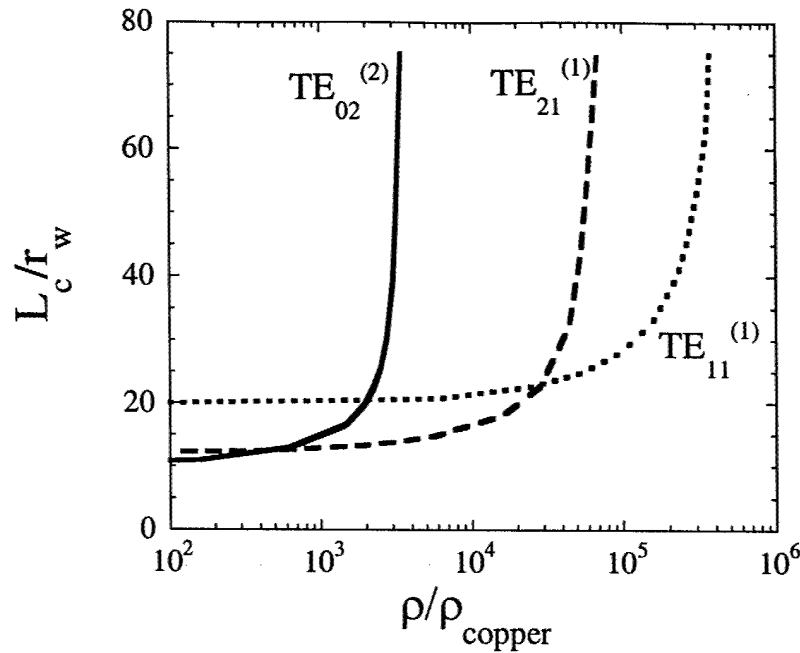


Fig. 3. Dependence on wall resistivity of the critical length for gyro-BWO in the $TE_{11}^{(1)}$, $TE_{21}^{(1)}$, and $TE_{02}^{(2)}$ modes (100 kV, 5 A, $v_{\perp}/v_z = 1.0$, $B/B_g = 1.0$, $r_c/r_w = 0.45$).

To produce the required attenuation, the wall of the interaction waveguide was coated with Aquadag, a resistive carbon colloid often used to discharge electron build-up on CRT screens. Aquadag had also been used in the ultrahigh gain TE_{11} gyro-TWT at NTHU. Acheson, the manufacturer, reports that Aquadag's resistivity usually falls in the range of $(36,000 - 80,000)\rho_{Cu}$, an extent that includes our desired value. The value reported by NTHU was $36,000\rho_{Cu}$. The actual value depends on the preparation and application method.

There was some concern because the material can alter the cutoff frequency due to its finite thickness. Therefore, HFSS was employed to determine the optimum thickness and resistance of the lossy material. HFSS models the loss layer as a semiconductor. It was found, however, that the attenuation is not dependent on the value of the dielectric constant. Figure 4 shows that the loss increases with the material's thickness, but it is unproductive to make the thickness greater than the skin depth. The primary effect of making it any thicker is to alter the effective cutoff frequency. For a resistivity of $70,000\rho_{Cu}$, the skin-depth at 94 GHz is 0.057 mm. Since it is desired that the loss layer not alter the cutoff frequency by more than a few percent, the

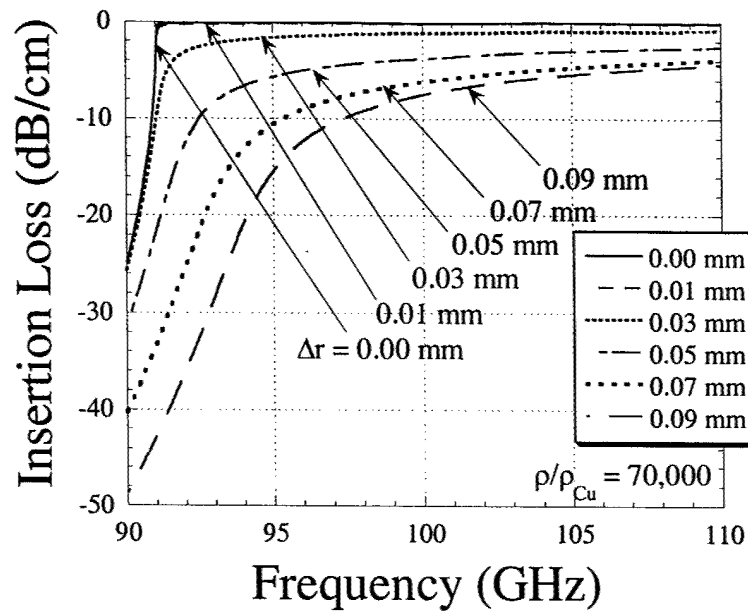


Fig. 4. Dependence on frequency of insertion loss for TE₀₁ waves through circuit loaded with a semiconductor liner for several values of thickness ($r_w=2.01$ cm, $\rho=70,000\rho_{Cu}$). The loss for $\Delta r = 0.01$ mm is nearly indistinguishable from the unloaded case.

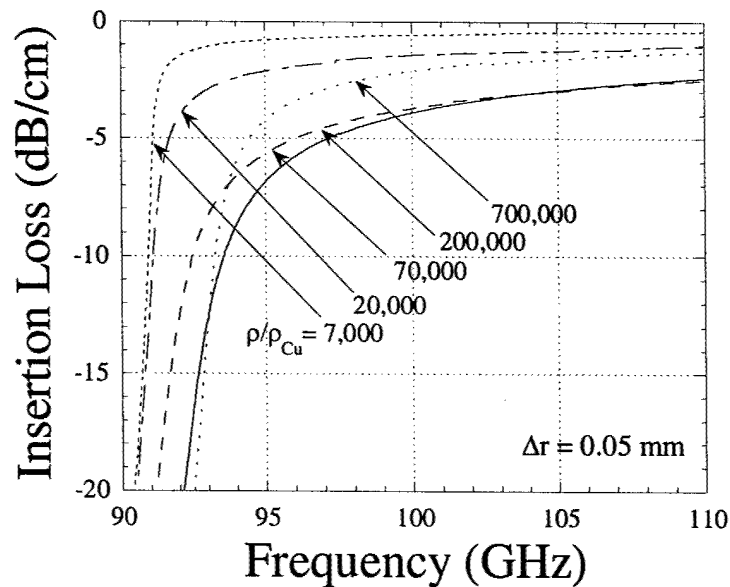


Fig. 5. Dependence on frequency of insertion loss for TE₀₁ waves through circuit loaded with a semiconductor liner for several values of resistivity ($r_w=2.01$ cm, $\Delta r=0.05$ mm).

thickness should not exceed a few percent of the wall radius. Figure 5 shows that for a thickness of 0.05 mm, the highest attenuation occurs for a resistivity in the range of $70,000\rho_{\text{Cu}}$ - $200,000\rho_{\text{Cu}}$. If the resistivity is any greater, then the loss is reduced because the thickness is significantly less than a skin depth, as is seen to occur for $\rho = 700,000\rho_{\text{Cu}}$.

The desired effective wall resistivity of $\rho/\rho_{\text{Cu}} = 70,000$ was achieved by coating the first 12 cm of the interaction circuit with sixteen layers of Aquadag. Through trial and error, by varying the dilution ratio with water, the precise value needed to suppress the $\text{TE}_{21}^{(1)}$ gyro-BWO mode was attained. Figure 6 compares the measurements of our final Aquadag-loaded circuit to our HFSS simulation of several appropriate cases. It is seen that the measurements of the lossy circuit agree well with the HFSS simulation of transmission through 12 cm of copper waveguide loaded with a 0.05 mm thickness semiconductor tube with a resistivity of 70,000 times copper. Furthermore, both agree with the HFSS simulation of transmission through 12 cm of unloaded metallic waveguide, whose resistivity is 70,000 times copper, which is the case that had been found to suppress the $\text{TE}_{21}^{(1)}$ gyro-BWO (Fig. 3). Specifically, the loss was measured to be 90 dB at 93 GHz, as desired.

By solving for the second order correction to the first order solution of the lossy gyro-TWT dispersion relation through the method of iteration, it was shown in the early 1980's that a gyro-TWT's gain is reduced by only one third of the circuit's insertion loss. This is because the bunched electron beam carries along the imprint of the wave. Therefore, the maximum loss rate that can be added to the circuit is equal to a factor of three times larger than the interaction growth rate in the circuit without loss. The UCD TE_{01} Gyro-TWT was designed to operate with a loss rate slightly larger than the predicted lossless interaction growth rate. The loss rate at 93 GHz is 7.5 dB/cm and the unloaded growth rate is 6.9 dB/cm.

Our self-consistent nonlinear particle-tracing code was modified so that it includes distributed wall loss and then employed to evaluate the large-signal characteristics of the amplifier. The code also includes reflections from the finite mismatch of the input and output couplers and the loss taper. The amplifier parameters are given in Table I. So that the wave is

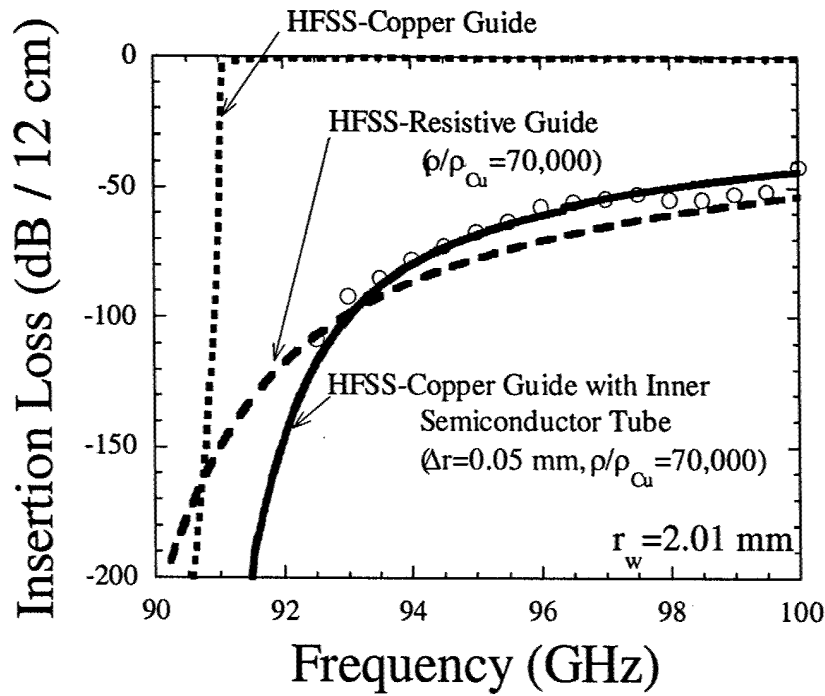


Fig. 6. Dependence on frequency of TE₀₁ mode's insertion loss through 12 cm length circuit from HFSS simulation (curves) and measurement (symbols). The broken curve shows the HFSS predictions for a semiconductor tube with a resistivity 70,000 times copper within copper waveguide. The unbroken curves are the predictions for a metallic waveguide with the resistivity of copper and 70,000 times copper.

Table I. Design Parameters of the TE₀₁ gyro-TWT amplifier.

Voltage	100 kV
Current	5 A
$\alpha = v_{\perp}/v_z$	1.0
$\Delta v_z/v_z$	5%
Magnetic Field, B_0	35.6 kG
B_0 / B_g	0.995
Cutoff Frequency	91.0 GHz
Wall Resistivity	70,000 ρ_{Cu}
Guiding Center Radius, r_c	0.45 r_w
Circuit Radius, r_w	0.201 cm
Copper Circuit Length	2.5 cm
Total Circuit Length	14.5 cm

not damped in the high power region, there is no loss added to the final 2.5 cm of the circuit and the loss in the preceding 1 cm is linearly tapered. When it is equipped with the proper collector and cooling, this would allow the device to operate continuously at an average power of 140 kW with only 50 W/cm² peak wall loading, well below the typical upper limit of 1 kW/cm² for CW gyrotrons, albeit with all-metal surfaces. The power handling capability of Aquadag is not known for sure, but it is likely that it can handle this load since it is regularly baked at 200 °C as part of its normal curing process. Furthermore, Aquadag combined with iron has been successfully used in severals of high average power coupled-cavity TWT's. The use of a relatively thick annulus of lossy ceramic so that it corresponds to the outer lobe of the TE₀₂ mode as employed in the circuit of the recent NRL TE₀₁ gyro-TWT is another method for distributing the required loss and handling the high power. Figure 7 shows the axial profile of the convective power growth in the amplifier. There is an inflection point near the beginning of the unloaded region where the growth rate increases. Theory indicates that a gyro-TWT's gain will decrease by one third of the added loss. Although the loss reduces the growth rate, it was found to have little effect on the efficiency. For an axial velocity spread of $\Delta v_z/v_z = 5\%$, the predicted peak power is 140 kW with an efficiency of 28% and a saturated bandwidth of 5%, as shown in Fig. 8. The large-signal gain is 50 dB, even though the circuit has 90 dB of loss at the frequency of 93 GHz.

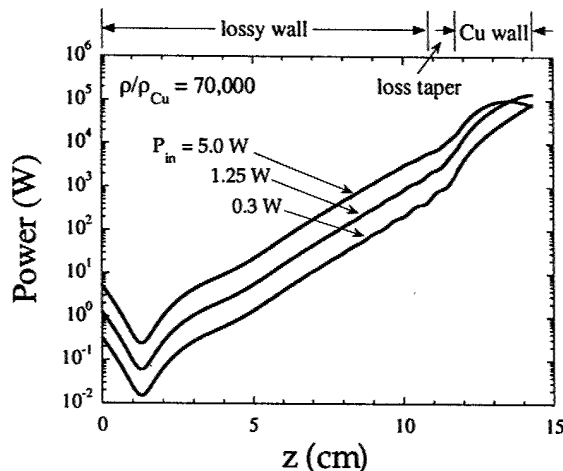


Fig. 7. Axial power growth of 92.25 GHz wave in the loaded TE₀₁ circuit for three values of input power [Table I].

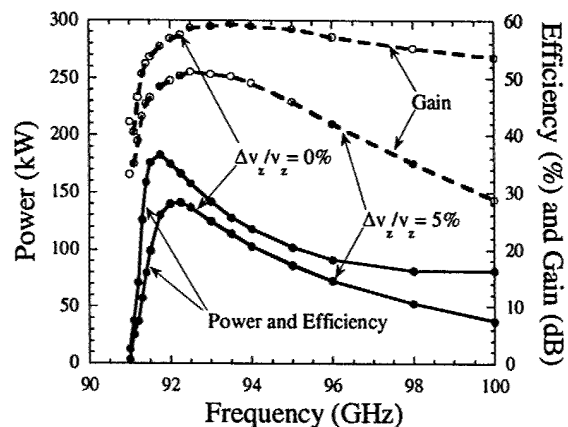
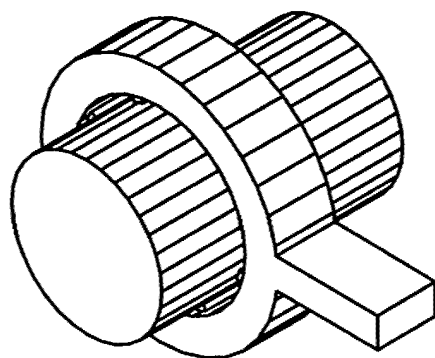
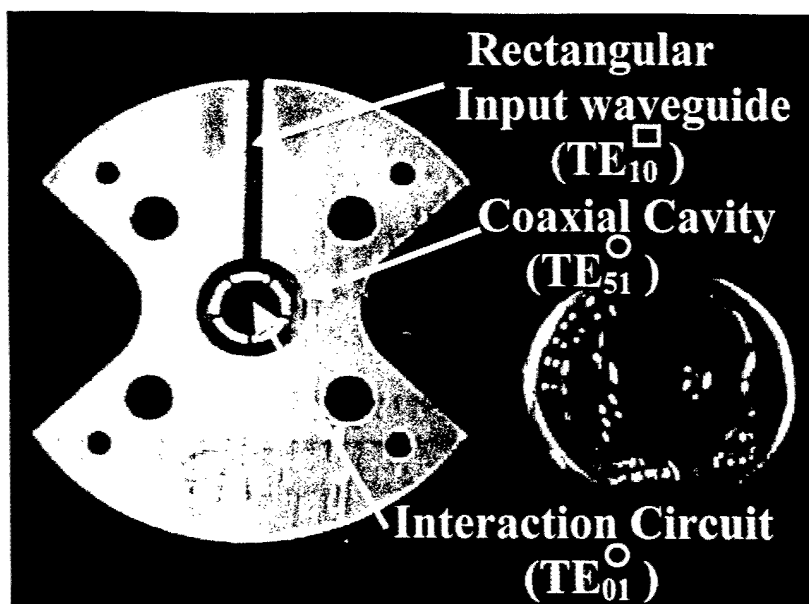


Fig. 8. Saturated bandwidth of the output power (unbroken line), efficiency (unbroken line) and gain (broken line) for an axial velocity spread of 0% and 5% [Table I].



(a)



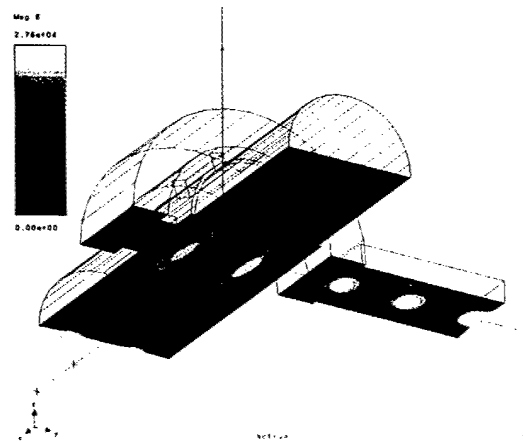
(b)

Fig. 9. (a) Schematic and (b) photograph of the TE₀₁ coaxial-filter input coupler.

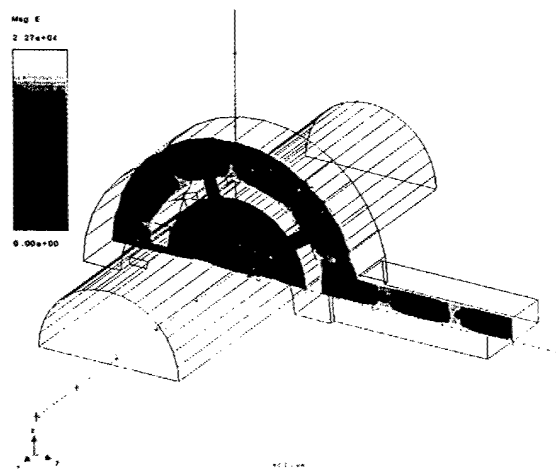
The coaxial-filter input coupler was designed with HFSS. As shown in Fig. 9, the input signal is injected from conventional rectangular waveguide into the coaxial TE₅₁ mode of a coaxial cavity and then into the desired TE₀₁ mode of the cylindrical interaction waveguide within the inner coax through five slots in the wall. Figure 10 shows the input and coupled waves from HFSS in two planes. In Fig. 10(a), the effect of the upstream short is evident. The short is merely a radial discontinuity one quarter wavelength upstream in the drift tube to cutoff and reflect the wave. Further upstream is an annular load to terminate the circuit. In this way, the coupler is a good match for all modes. From the symmetry of the wave pattern in Fig. 10(b), it is clear that a TE₅₁ wave in the coaxial cavity is coupling to a TE₀₁ wave in the inner waveguide.

Figure 11 compares the measured coupling with the HFSS predictions. Whereas HFSS predicts greater than -1 dB coupling over a 3% bandwidth, the input coupler actually exhibits a minimum of -2 dB coupling over this bandwidth. The input coupler's performance is limited by the 96.5 GHz cutoff of the upstream short. The discontinuity in the bandwidth can be shifted to higher frequency by reducing the inner diameter of the short. Figure 11 also shows the wider bandwidth predicted for a design with a short with a slightly reduced diameter and where the

resonant frequency of the coaxial cavity has been increased to 95 GHz from 94 GHz. Although the modified coupler's predicted bandwidth of 7% is much more suitable for the amplifier's predicted bandwidth of 5% (Fig. 8), the initial hot tests have employed the former design, since good transmission of the electron beam has been a more important concern in the early experiments. A similar, lower coupling transducer monitors the output power.



(a)



(b)

Fig. 10. Intensity of electromagnetic waves in the TE_{01} coaxial-filter input coupler from HFSS, showing (a) an axial view cut through the axis and (b) a cross-sectional view through the coaxial cavity.

To achieve the wide bandwidth predicted by theory (Fig. 8), it is crucial that the electron beam has a low velocity spread. Two single-anode MIG electron guns have been designed using EGUN for the gyro-TWT program. . Since the experiments employing the original gun yielded a narrow bandwidth and low levels of output power, which indicated that the velocity spread was high, a modified MIG was built with slanted inner and outer focusing electrodes. For a 100 kV, 5 A electron beam with $v_{\perp}/v_z = 1.0$, the predicted axial velocity spread of the new gun is only 2.2 %. Both of these MIGs have a very large cathode angle of 74° . For large cathode angles, the design rules change. It is no longer necessary to keep the gap between the inner and outer electrodes larger than twice the Larmor radius. The geometry becomes less coaxial and more planar. Our dispenser cathodes have been manufactured by Spectramat. The edges of the emitting strip have been coated with Molybdenum to suppress edge emission.

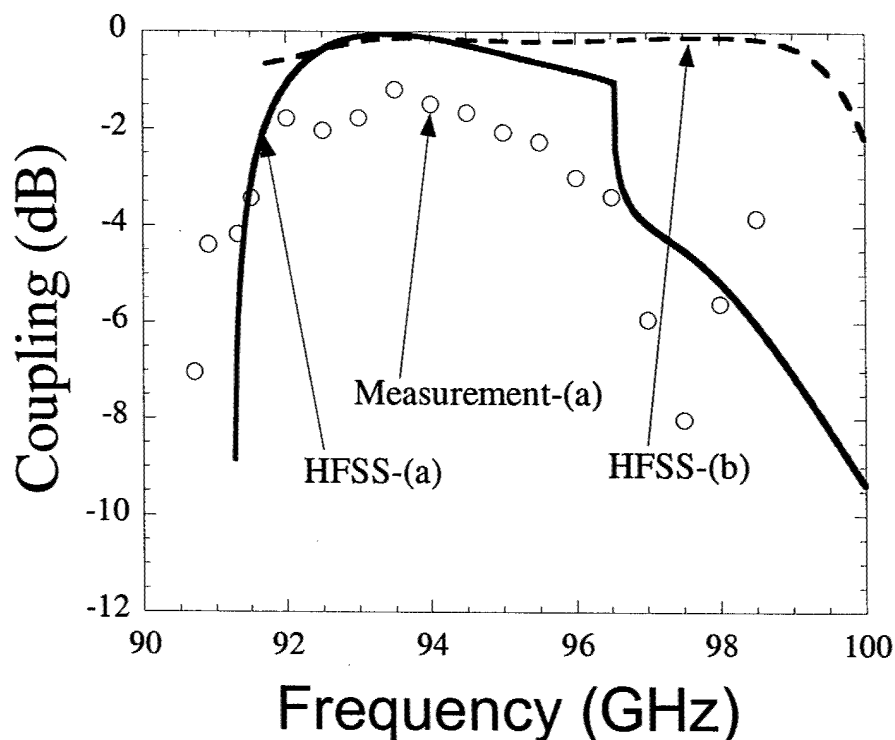


Fig. 11. Bandwidth of the insertion loss through the TE_{01} coaxial-filter input coupler from measurement and HFSS and for the modified coupler from HFSS.

5.1.3 Experimental Measurements

The UCD single-stage heavily loaded W-Band gyro-TWT has been tested at full RF input power using a 100 W folded waveguide TWT driver with a bandwidth of 5%. . As mentioned above, the results with the original MIG were disappointing. The narrow bandwidth and low output power indicated that the axial velocity spread of the electron beam was about 10% rather than the design value of 5%. This motivated the design and fabrication of a new MIG electron gun. The modified MIG employs the same dispenser cathodes; however, the electrodes immediately inside and outside of the emitter are now slanted to give better focusing. EGUN simulations predict that the axial velocity spread is only 2.2%. This immediately resulted in record level performance. Preliminary hot test measurements, made at lower voltage than the design value of 100kV, yielded 53kW saturated power with 47dB gain, 14% efficiency, and 1.1% bandwidth. Significantly higher performance is anticipated as the device is optimized.

The high voltage modulator used to drive the electron gun is capable of producing 50 A at 100 kV (2 k Ω) and is shown in Fig.12. A HV step-up transformer boosts by a factor of ten the voltage pulse produced by a pulse-forming network. Since the MIG represents a relatively high impedance (20 k Ω), a 2 k Ω resistor has been placed in the oil tank to terminate the circuit and absorb most of the pulse's energy.

The RF input source to drive our test amplifier into saturation is a Hughes 100 W W-Band folded waveguide TWT with a bandwidth of 5 %. Our colleagues at SLAC collaborated with us to build the 25 kV mod anode pulser needed to drive the input amplifier. The UCD-SLAC HV modulator is shown in Fig. 13 along with the test stand for the W-Band TWT. The modulator is sufficiently versatile that it can also be used to drive our other W-Band source, a 2 kW EIO with a tuning range of 5 %.

The test device is a copious generator of millimeter wave emission. The properties of these oscillations, especially the gyro-BWO, will be studied in depth in the future. However, there are regions where the device is quiet and gives good amplifier characteristics. Figure 14 shows the typical pulse traces of the beam voltage, beam current, wave input power and wave output power. Although the gyro-TWT was designed for 100 kV, it has operated well at lower voltage. The stability of the test device is evidenced in Fig 15, which shows the amplifier's transfer curve. For a 64 kV, 6.0 A electron beam, the output reaches 53 kW at 92.2 GHz with a

magnetic field of 34.2 kG, which corresponds to an efficiency of 14%. The small-signal gain is 50 dB and the large-signal gain is 47 dB. The new amplifier yields a saturated bandwidth of 1.1 %, as shown in Fig. 16. Since the roll-off of the bandwidth at $\cong 96.5$ GHz is determined by the coupler (see Fig. 11), an appreciably wider bandwidth can be expected when the current input coupler is replaced by the modified input coupler. The modified coupler has been built and cold tested. The measured transmission properties shown in Fig. 17 verify that the fall-off has been increased from the current value of 96.5 GHz to 100 GHz. Swapping the couplers is the next task planned for the project.

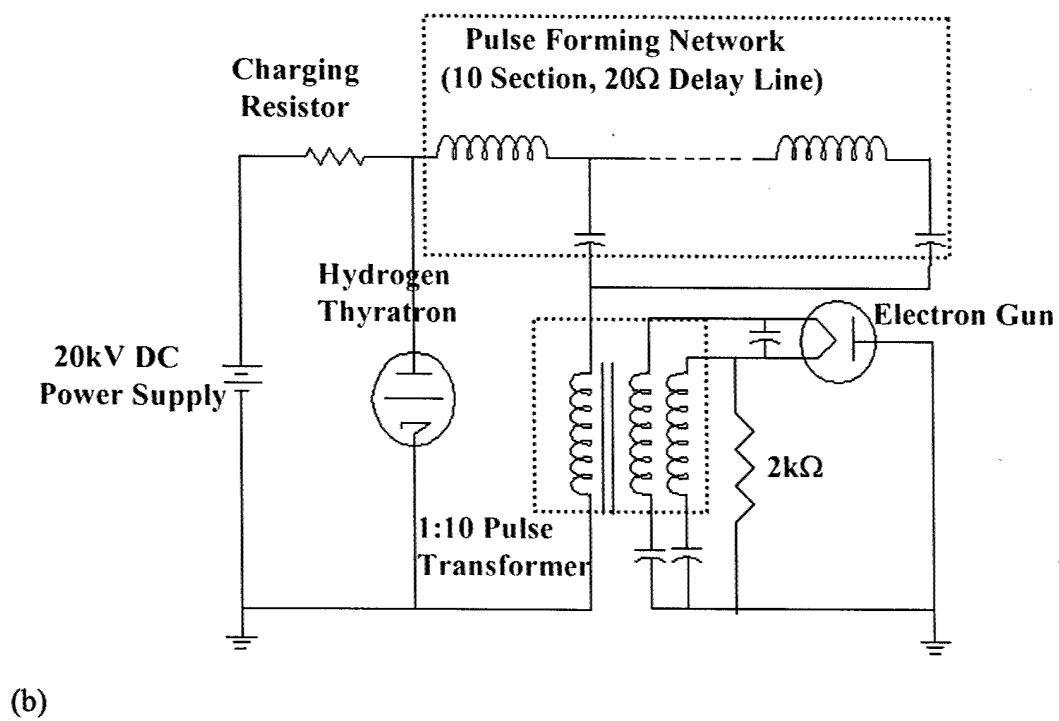
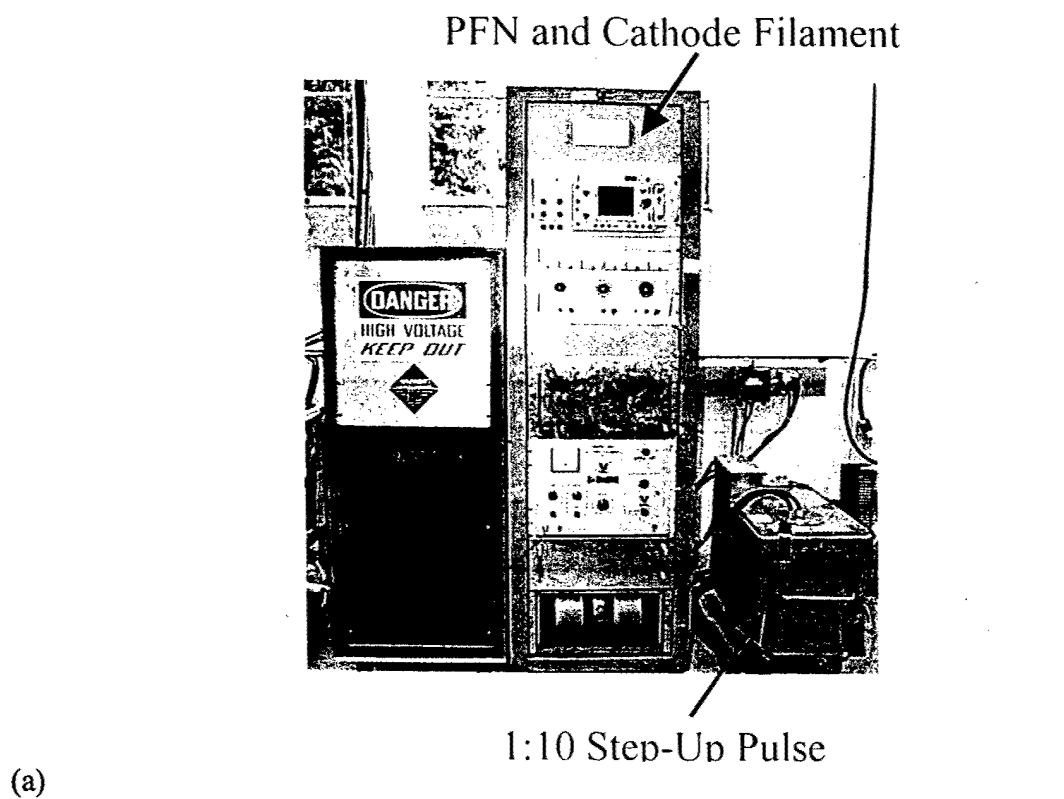
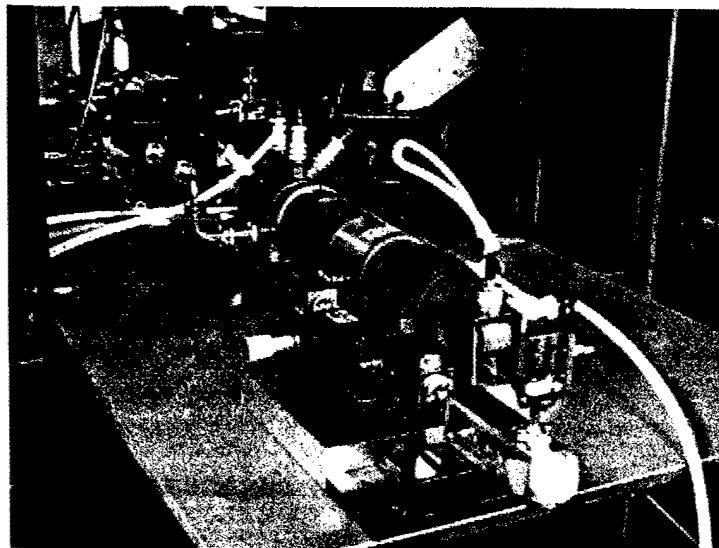


Fig. 12. High voltage modulator (a) photograph and (b) schematic.



(a)



(b)

Fig. 13. Photographs of (a) the UCD-SLAC W-Band modulator and (b) the Hughes 94 GHz, 100 W folded waveguide TWT.

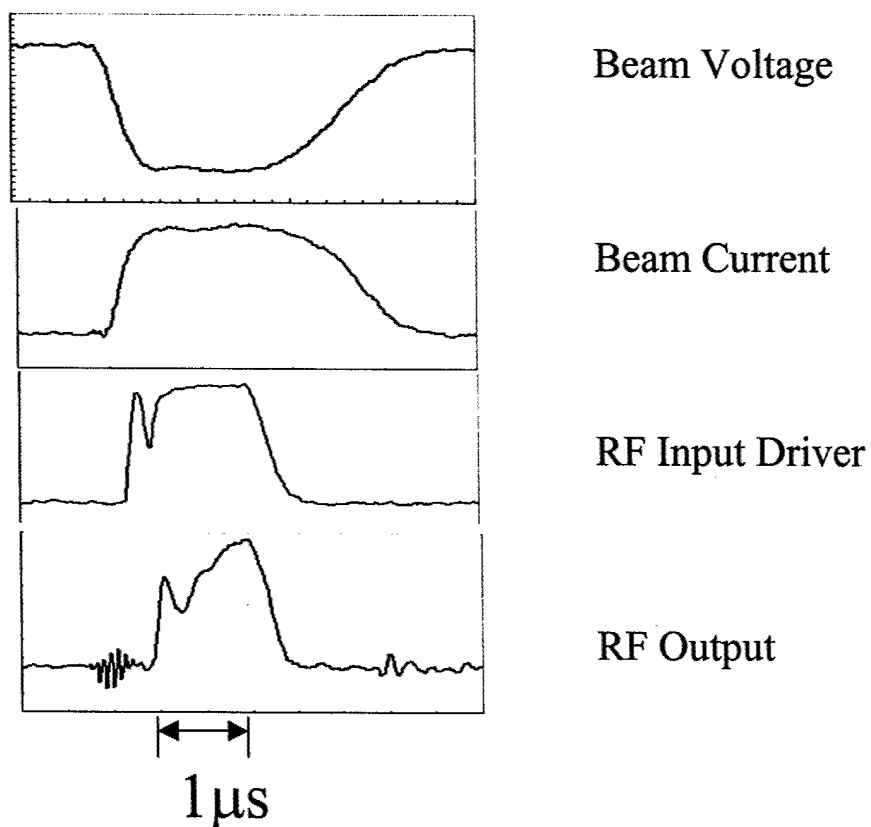


Fig. 14. Typical oscilloscope traces of the beam voltage, beam current, RF input power, and RF output power.

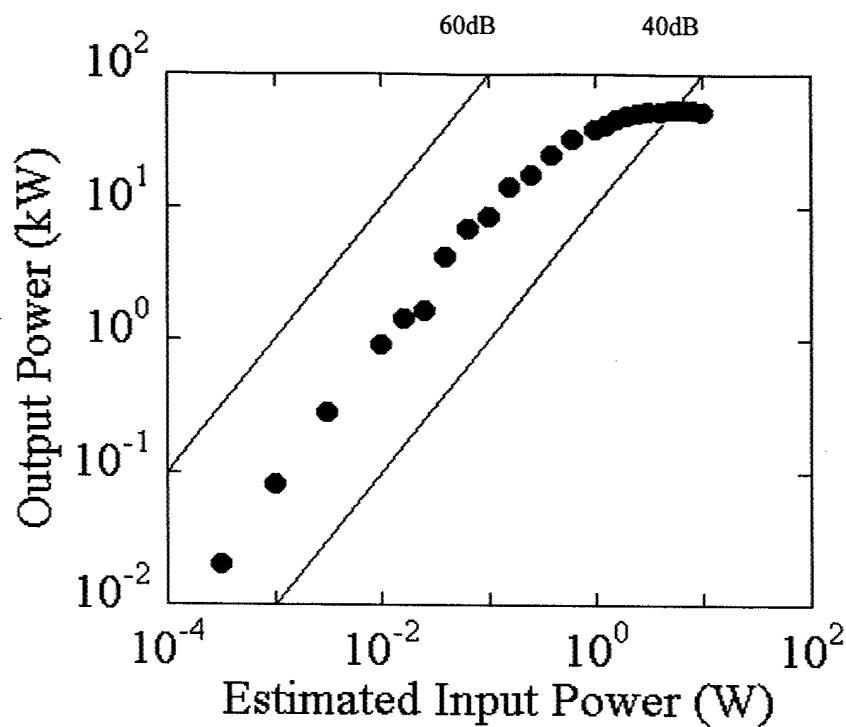


Fig. 15. Measured output power versus input power (63 kV, 6.0 A, 34.2 kG, 92.2 GHz).

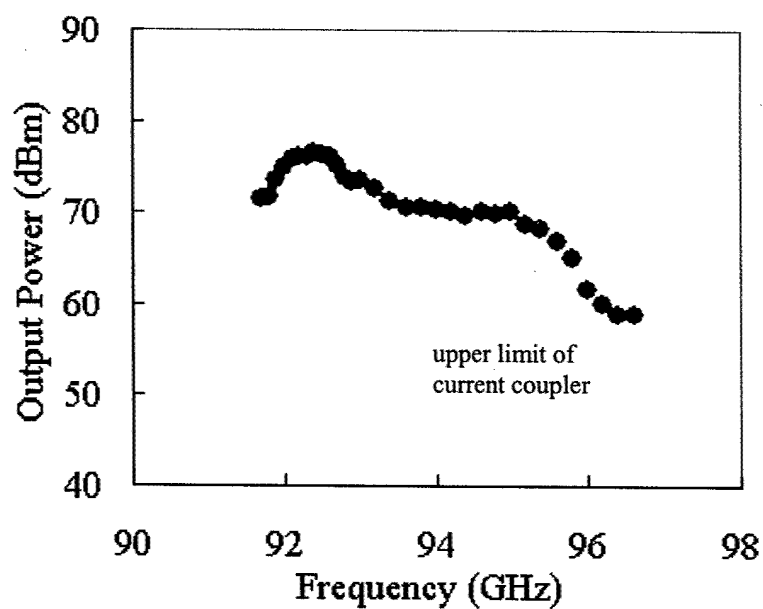


Fig. 16. Measured output power versus frequency under saturated operation.

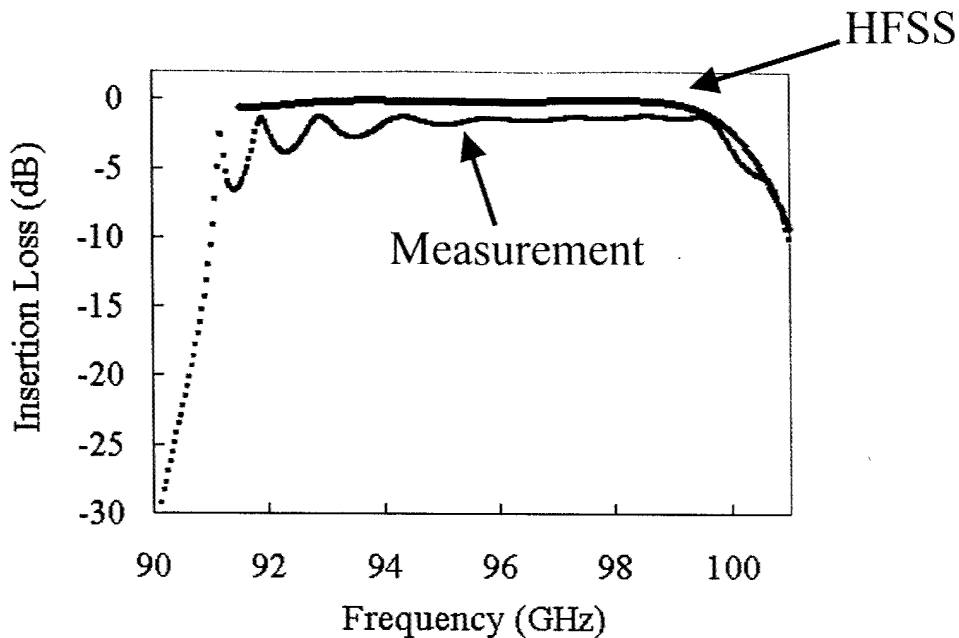


Fig. 17. Bandwidth of the insertion loss for the modified coaxial coupler from measurement and HFSS.

5.2 TE_{01} Gyro-BWO

5.2.1 Design

A high power, W-Band gyro-BWO with broad bandwidth is also being developed. For high average power, the UCD gyro-BWO employs an unloaded, low loss TE_{01} circuit. The TE_{01} gyro-BWO experiment will utilize many components from the TE_{01} gyro-TWT experiment. Since the circuit is sufficiently short that only the TE_{01} mode need be considered, the simplified dispersion diagrams shown in Fig. 18 are relevant. In a gyro-BWO, the wave grows counter to the propagation direction of the electron beam. The intensity of the generated wave is maximum at the electrons' entrance to the circuit. The frequency can be varied electronically by more than 10%. Our dual-mode gyro-BWO has fast frequency tuning by changing the beam's voltage or α (v_{\perp}/v_z) as seen in Fig. 18(a) and slow tuning by changing the amplitude of the magnetic field as seen in Fig. 18(b).

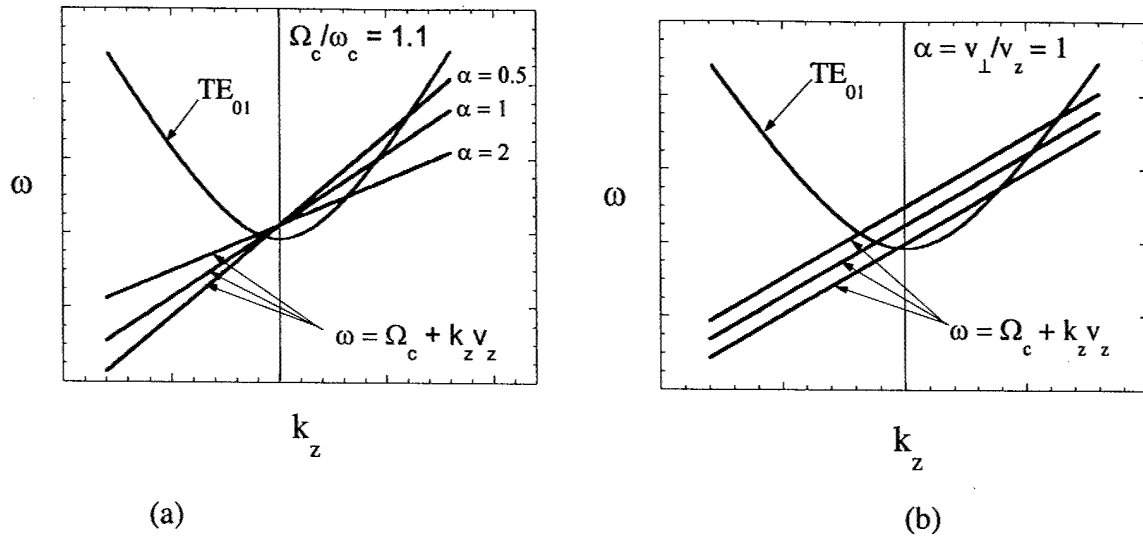


Fig. 18. Dispersion relation of the TE₀₁ gyro-BWO with frequency tuning by changing (a) $\alpha = v_{\perp}/v_z$ and (b) magnetic field amplitude.

Table II. Design parameters of the tapered TE₀₁ gyro-BWO.

Voltage	100 kV
Beam Current	5 A
$\alpha = v_{\perp}/v_z$	1.0
$\Delta v_z/v_z$	5%
Magnetic Field, B_0	43 kG
B_0 / B_g	1.2
Guiding Center Radius, r_c	0.45 r_w
Input Circuit Radius	0.201 cm
Output Circuit Radius	0.189 cm
Circuit Length	4.7 cm

We have used a self-consistent slow-timescale particle-tracing simulation code to evaluate the device. The parameters are given in Table II. The TE_{01} gyro-BWO driven by a 100 kV, 5 A electron beam with $v_{\perp}/v_z = 1$ is predicted to generate 100 kW with 20% efficiency and 10% bandwidth, as shown in Fig. 19.

Figure 20 shows a schematic of the gyro-BWO circuit. To enhance the efficiency by improving the bunch formation, the inner diameter of the circuit is tapered by 6%. Both ends of the circuit are terminated yielding minimal reflections. The generated rf power is extracted from the TE_{01} coax coupler on the upstream end of the circuit nearest the MIG. The downstream end is terminated in an rf load. The device has been fabricated. The circuit is shown in Fig. 21. The TE_{01} gyro-BWO will be tested immediately after the initial tests of the TE_{01} gyro-TWT.

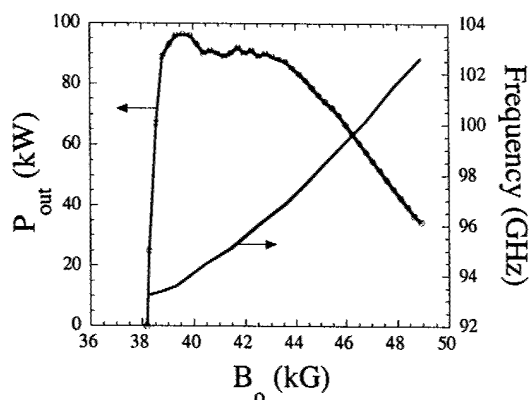


Fig. 19. Dependence on magnetic field of the output power and frequency (TE_{01} , 100 kV, 5 A, $v_{\perp}/v_z=1$, $r_c/r_w=0.45$, Table II).

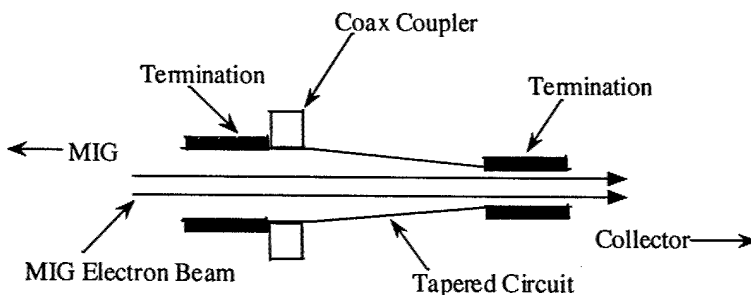
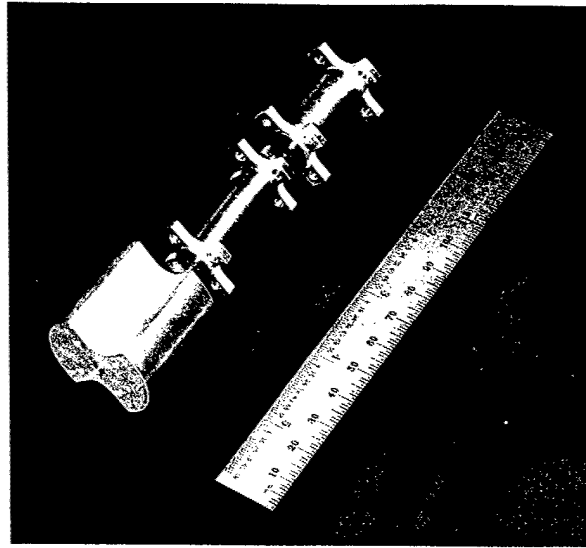
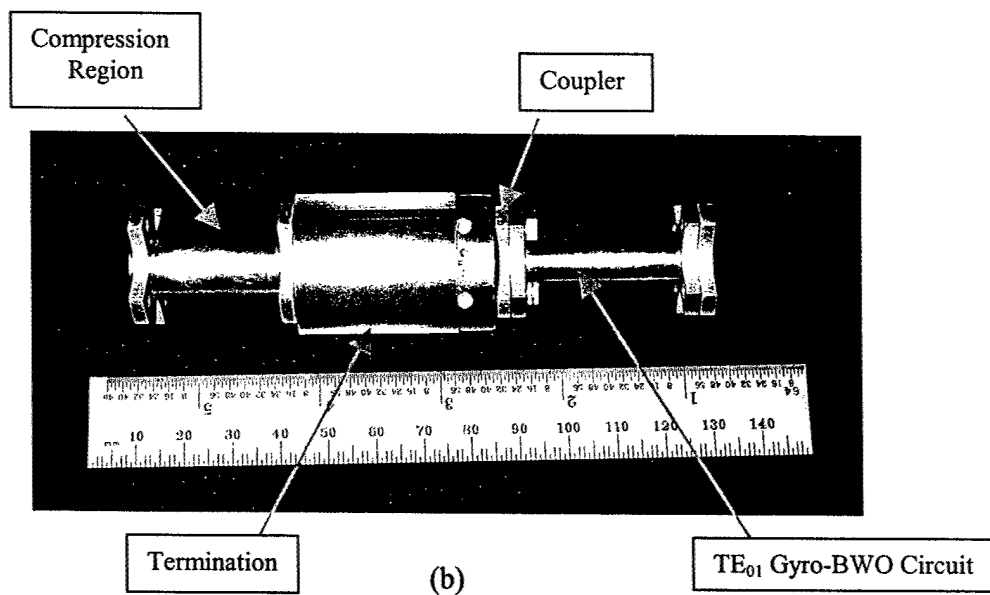


Fig. 20. Schematic of the TE_{01} gyro-BWO.



(a)



(b)

Fig. 21. Photographs of the TE₀₁ gyro-BWO circuit, showing (a) partial and (b) complete circuit.

5.2.2 Theory -- Start-Oscillation Current of Lossy Gyro-BWO

We have also investigated the gyro-BWO start oscillation current in order to explain the observed high power emission from our lossy amplifier circuit when the magnetic field is raised above the operating value. The method of equivalence is used to calculate the gyro-BWO start oscillation current in the presence of loss. The gyro-BWO starting current is determined from the well known equation for the linear BWO by replacing the linear BWO parameters by equivalent gyro-BWO parameters (R.W.Grow et al., IEEE Trans. on Electron Devices, Vol. ED-17, No.12, December, 1970; and M.Caplan, "An Application of the Relativistic Bunching of Electrons to the Generation of Intense Millimeter Microwave Radiation," UCLA Ph.D dissertation, 1986). The equivalent interaction parameters for the two devices are listed in Table III.

Table III Equivalent interaction parameters for linear BWO and gyro-BWO

Parameter	Linear BWO	Gyro-BWO
Gain parameter	$C = \left(\frac{Z_0 I_0}{4V_0} \right)^{\frac{1}{3}}$	$C_g = \left(\frac{k_c^4}{2k_b^4} I_b F_{mn} \epsilon_v \right)^{\frac{1}{3}}$
Synchronism parameter	$b = \frac{1}{C} \left(\frac{u_0}{v_p} - 1 \right)$	$g = \frac{k_g - k_b}{k_b C_g}$
Loss parameter	$d = 0.0184 \frac{L}{C}$	$d = 0.0184 \frac{L}{C_g}$

Symbol Key for Table III

Z_0 : circuit impedance

V_b : beam voltage

v_p : phase velocity

k_c : cutoff wavenumber (ω_c/c)

k_g : waveguide wavenumber

I_b : beam current

u_0 : beam velocity

L : loss per wavelength

k_b : beam wavenumber ($(\omega - \Omega)/v_z$)

$$F_{mn} = \frac{J_{1-m}^2(k_{mn} R_g/a)}{k_{mn}^2 J_m^2(k_{mn})(1 - m^2/k_{mn}^2)}$$

$$\epsilon_v = \frac{2.348 \times 10^{-4}}{\gamma \beta_z} \left(\frac{\beta_{\perp}}{\beta_z} \right)^2 \left(J_1 \left(\frac{\beta_{\perp} \omega_c}{\Omega_c} \right) \right)^2$$

By combining Eq.(1) used in linear BWO and Eq.(2) used in GyroBWO (by setting $C_{st}=C_g$),

$$C_{st}=0.012 \frac{L_{db}}{N} \left(1 + \frac{1013}{L_{db}^2} \right) \text{-----} (1)$$

$$C_g = \left(\frac{k_c^4}{2k_b^4} I_b F_{mn} \epsilon_v \right)^{\frac{1}{3}} \text{-----} (2)$$

where L_{db} is the total loss of the circuit and N is the circuit length in wavelengths, the start oscillation current for gyro-BWO in a lossy circuit can be expressed as Eq.(3).

$$I_s = \frac{2k_b^4}{F_{mn} \epsilon_v k_c^4} \left(0.012 \frac{L_{db}}{N} \right)^3 \left(1 + \frac{1013}{L_{db}^2} \right)^3 \text{-----} (3)$$

Figure 22 shows the dispersion diagram for the $TE_{01}^{(1)}$ Gyro-TWT when the magnetic field is raised 12% above grazing. The $TE_{11}^{(1)}$, $TE_{21}^{(1)}$, $TE_{01}^{(1)}$ and $TE_{02}^{(2)}$ gyro-BWO modes occur when the first and second cyclotron resonance lines intersect the waveguide dispersion curves for negative k_z . Only the case of synchronism is considered here ($g=0$ or $k_b=k_g$). Table IV shows the calculated start oscillation current values for different values of B_o/B_g for the $TE_{01}^{(1)}$ mode in our circuit with $L_{db}=100\text{dB}$. Since I_s is proportional to k_b^4 , the starting current is seen to increase strongly with k_b . The strongest interaction and lowest starting current occurs when the circuit cutoff is excited ($k_b=0$). These values agree with our measurements. Starting currents in the range of 1-5 A are measured. Figure 23 shows that the starting current is also a strong function of the loss. It should be pointed out that the theory makes the approximation that the loss is independent of frequency. We plan to incorporate a more realistic frequency dependence in the theory in the future. Figure 24 shows the calculated start oscillation current versus loss for the four modes. Since I_s is proportional to k_b^4 , the $TE_{01}^{(1)}$ mode which intersects closest to cutoff shows the lowest I_s . Figure 25 shows that a gyro-BWO oscillates easier at lower voltage. This is because slower electrons spend more time in the circuit. Figure 26 shows that a gyro-BWO

oscillates easier for higher alpha (v_{\perp}/v_z), which is because the transverse velocity is driving the interaction. Both Figs. 25 and 26 show that a gyro-BWO is more stable as the magnetic field is increased above grazing ($B_g=1$).

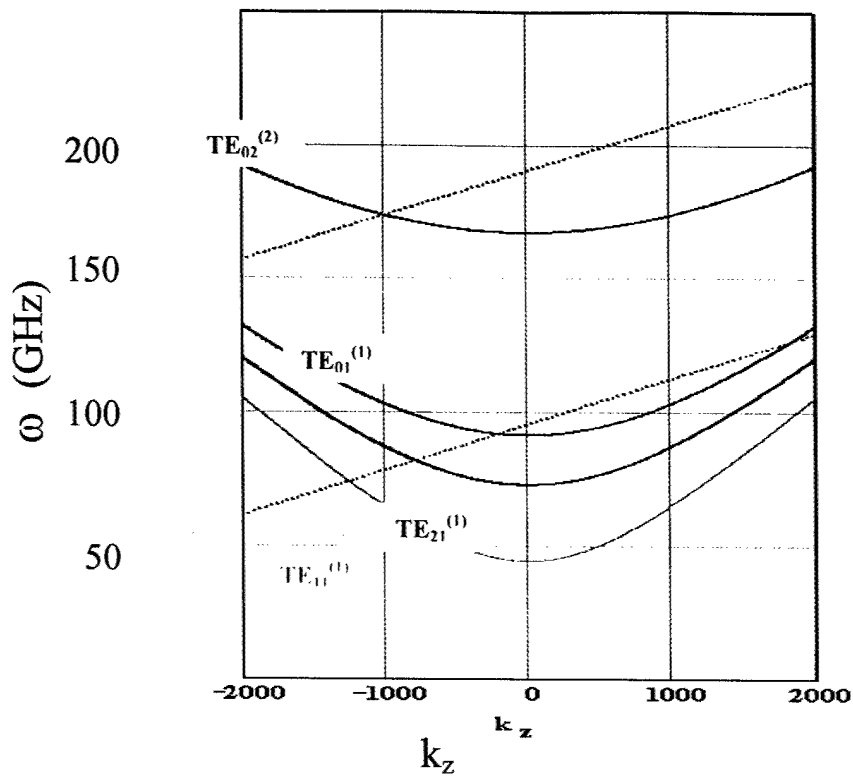


Fig. 22. Dispersion diagram for $TE_{01}^{(1)}$ gyro-BWO [$V_b=80\text{kV}$, $\alpha=1.0$, $B_o/B_g=1.118$].

Table IV. The dependence of the $TE_{01}^{(1)}$ gyro-BWO start oscillation current and the propagation constant on the magnetic grazing value for $\alpha=1.0$, $V_b=80\text{kV}$ and $L_{db}=100\text{dB}$

B_o/B_g	$k_b(=k_g)/m$	I_s (A)
1.095	-119.8	0.372
1.098	-131.8	0.544
1.101	-143.7	0.769
1.104	-155.3	1.045
1.107	-166.9	1.394
1.110	-178.4	1.814
1.112	-189.6	2.307
1.118	-211.6	3.569
1.124	-233.1	5.237
1.129	-254.2	7.376
1.135	-274.8	10.024
1.141	-294.9	13.249
1.147	-314.7	17.091
1.152	-334.1	21.590

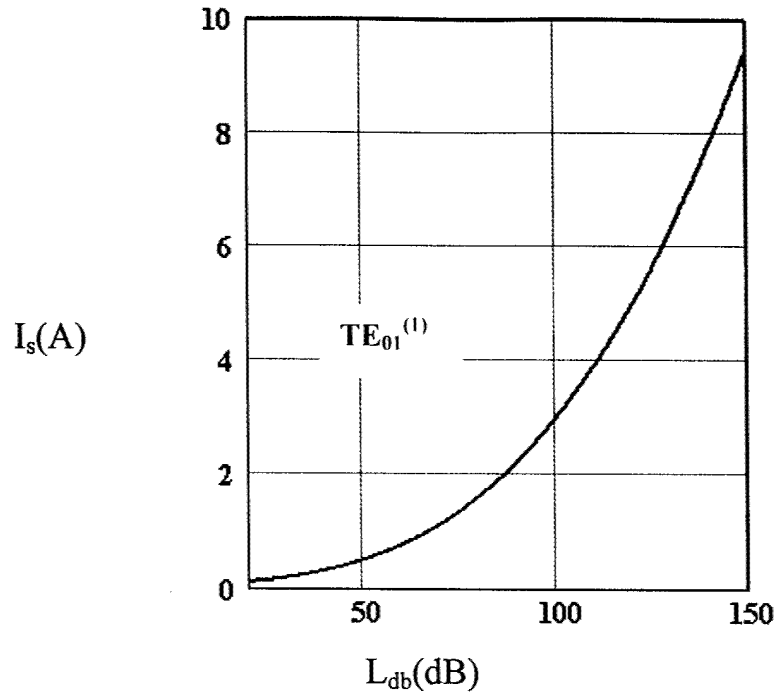


Fig. 23. The dependence of the $TE_{01}^{(1)}$ start oscillation current on circuit loss using Eq.(3) ($V_b=80\text{kV}$, $\alpha=1.0$, $B_o/B_g=1.118$).

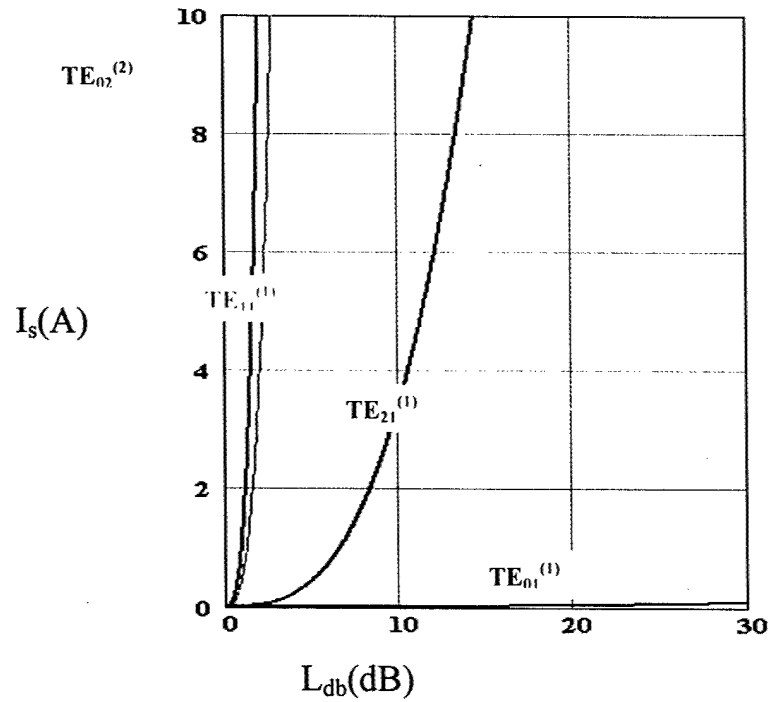


Fig. 24. The dependence on circuit loss of the start oscillation current for the $TE_{11}^{(1)}$, $TE_{21}^{(1)}$, $TE_{01}^{(1)}$ and $TE_{02}^{(2)}$ modes using Eq.(3) ($V_b=80\text{kV}$, $\alpha=1.0$, $B_o/B_g=1.118$).

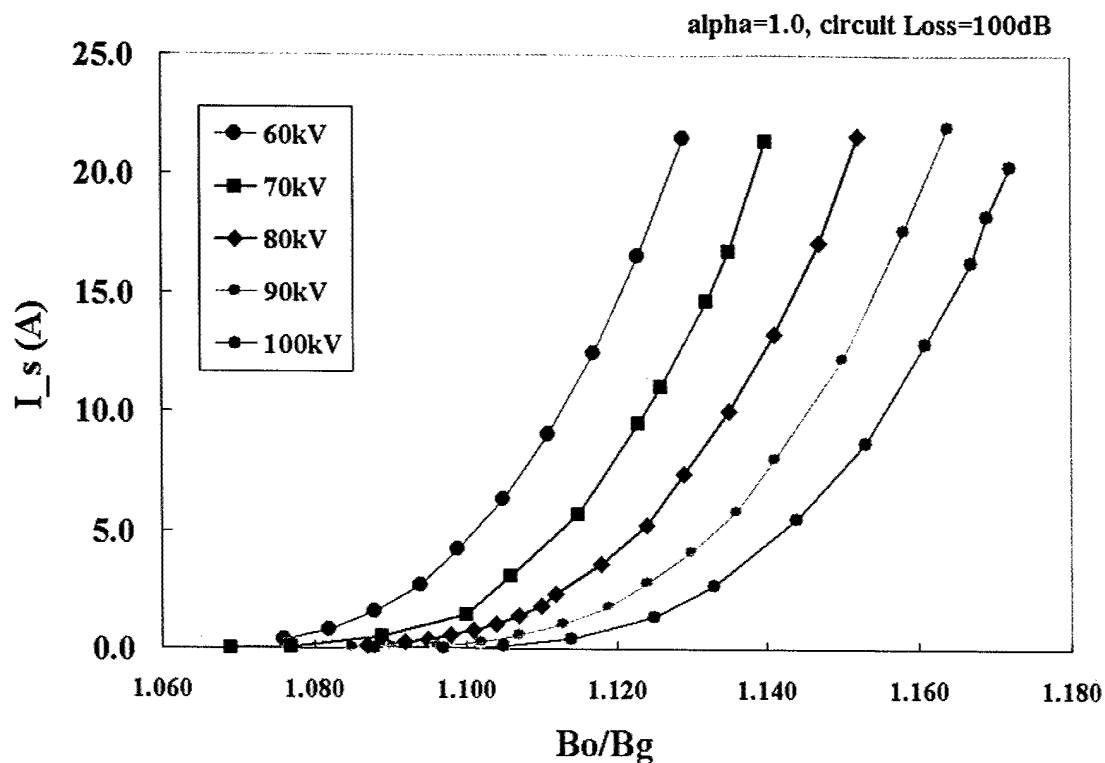


Fig. 25. The dependence of the start oscillation current (Eq. 3) on the magnetic grazing parameter for the $TE_{01}^{(1)}$ operating mode for several values of beam voltage ($\alpha=1.0$, $L_{db}=100$ dB).

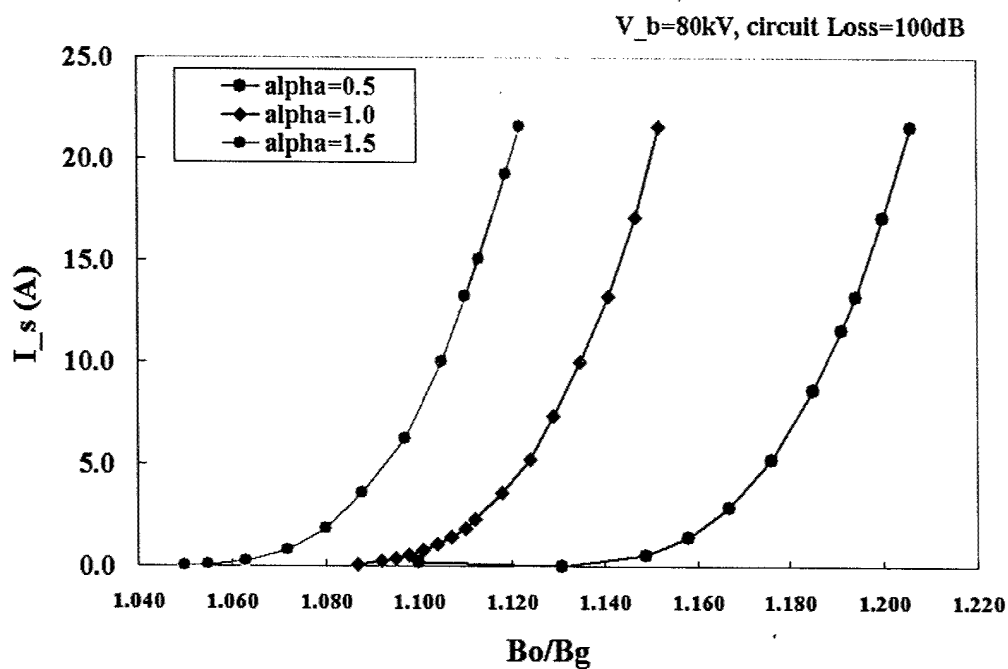


Fig. 26. The dependence of the start oscillation current (Eq. 3) on the magnetic grazing parameter for the $TE_{01}^{(1)}$ operating mode for several values of v_{\perp}/v_z ($V_b=80$ kV, $L_{db}=100$ dB).

6.0 Personnel

Dr. Neville C. Luhmann, Jr., Professor and Principal Investigator

Dr. David B. McDermott, (Initial Principal Investigator)

Ms. Heather H. Song, Graduate Student

Ms. Hsin-Lu Hsu, Graduate Student

Mr. Peter S. Marandos, Graduate Student

Mr. Jase S. Lee, Graduate Student

In addition, we have significantly benefited from the assistance of Dr. Larry Barnett, who has graciously volunteered his time.

7.0 Publications and Presentations

D.B. McDermott, H.H. Song, Y. Hirata, A.T. Lin, T.H. Chang, H.L. Hsu, K.R. Chu, and N.C. Luhmann, Jr., "Design of a High Power W-Band Heavily Loaded TE01 Gyro-TWT Broadband Amplifier," *IEEE Trans. on Plasma Science*, vol. 30, pp. 894-902, 2002.

"Gyrotron Oscillators and Amplifiers," V. L. Granatstein, G. Nusinovich, M. Blank, K. Felch, R. M. Gilgenbach, H. Guo, H. Jory, N. C. Luhmann, Jr., D. B. McDermott, J. Rodgers, and T. A. Spencer, to be published in "Advances in High Power Microwave Sources and Technologies," edited by R.J. Barker and E. Schamiloglu, IEEE Press, 2000.

Y. Hirata, D.B. McDermott, A.T. Lin, T.H. Chang, K.R. Chu, and N.C. Luhmann, Jr., "Heavily-Loaded W-Band TE01 Gyro-TWT," *Digest of 27th IEEE Int. Conference on Plasma Science*, p. 171, 2000.

Y. Hirata, D.B. McDermott, A.T. Lin, T.H. Chang, K.R. Chu, and N.C. Luhmann, Jr., "W-Band TE01 Gyro-TWT with Heavy Wall Loss," *Digest of 25th Int. Conference on Infrared and Millimeter Waves*, 2000.

D.B. McDermott, Y. Hirata, A.T. Lin, T.H. Chang, K.R. Chu, and N.C. Luhmann, Jr., "94 GHz Lossy TE₀₁ Gyro-TWT," *Bulletin of 42nd Meeting of APS Div. Of Plasma Physics*, 2000.

D.B. McDermott, H. Song, Y. Hirata, A.T. Lin, T.H. Chang, K.R. Chu, and N.C. Luhmann, Jr., "140 kW, 94 GHz Heavily Loaded TE₀₁ Gyro-TWT," *Digest of 2nd Int. Vacuum Electronics Conference*, 2001.

D.B. McDermott, H.H. Song, Y. Hirata, A.T. Lin, T.H. Chang, K.R. Chu, and N.C. Luhmann, Jr., "94 GHz Heavily Loaded TE₀₁ Gyro-TWT," *Digest of 27th IEEE Int. Conference on Plasma Science*, p. 515, 2001.

D.B. McDermott, H.H. Song, Y. Hirata, A.T. Lin, T.H. Chang, H.L. Hsu, K.R. Chu, and N.C. Luhmann, Jr., "Heavily-Loaded W-Band TE₀₁ Gyro-TWT," *Digest of 25th Int. Conference on Infrared and Millimeter Waves*, Toulouse, France, 2001.

D.B. McDermott, H.H. Song, Y. Hirata, A.T. Lin, T.H. Chang, H.L. Hsu, K.R. Chu, and N.C. Luhmann, Jr., "Stability of Heavily-Loaded W-Band TE₀₁ Gyro-TWT," *submitted to 43rd Meeting of APS Div. Of Plasma Physics*, Long Beach, CA, 2001.

D.B. McDermott, H.H. Song, Y. Hirata, A.T. Lin, T.H. Chang, H.L. Hsu, K.R. Chu, and N.C. Luhmann, Jr., "140 kW W-Band Heavily Loaded TE₀₁ Gyro-TWT Amplifier," *High Energy Density and High Power RF* (B.E. Carlsten, ed.), AIP Conference Proceedings, Fifth Workshop on High Energy Density and High Power RF, Snowbird, Utah, 2001.

D.B. McDermott, H.H. Song, Y. Hirata, A.T. Lin, T.H. Chang, H.L. Hsu, P.S. Marandos, J.S. Lee, K.R. Chu, and N.C. Luhmann, Jr., "High Power W-Band Heavily Loaded TE₀₁ Gyro-TWT," *Digest of 3rd Int. Vacuum Electronics Conference*, 2002.

D.B. McDermott, H.H. Song, Y. Hirata, A.T. Lin, T.H. Chang, H.L. Hsu, K.R. Chu, and N.C. Luhmann, Jr., "Design of a W-Band TE₀₁ Gyro-TWT with High Power and Broadband Capabilities," *Digest of 28th IEEE Int. Conference on Plasma Science*, 2002.

D.B. McDermott, H.H. Song, L.R. Barnett, Y. Hirata, A.T. Lin, H.L. Hsu, P.S. Marandos, J.S. Lee, T.H. Chang, K.R. Chu, and N.C. Luhmann, Jr., "High Power Broadband W-Band Gyrotron Traveling Wave Amplifier," *Digest of 26th Int. Conference on Infrared and Millimeter Waves*, 2002.

D.B. McDermott, H.H. Song, L.R. Barnett, Y. Hirata, T.H. Hsu, P.S. Marandos, J.S. Lee, T.H. Chang, K.R. Chu and N.C. Luhmann, Jr., "A Heavily Loaded W-Band TE₀₁ Gyro-TWT with High Power and Broadband Capabilities," *Bulletin of 44th Meeting of APS Div. Of Plasma Physics*, Orlando, FL, 2002.

H.H. Song, L.R. Barnett, D.B. McDermott, Y. Hirata, H.L. Hsu, P.S. Marandos, J.S. Lee, T.H. Chang, K.R. Chu, and N.C. Luhmann, Jr., "W-Band Heavily Loaded TE₀₁ Gyrotron Traveling Wave Amplifier" *Digest of 4th IEEE Int. Vacuum Electronics Conference*, 2003.

8.0 Patents

None

9.0 Honors

Dr. McDermott served as the Guest Editor for the IEEE Transactions on Plasma Science's Ninth Special Issue on High Power Microwave Generation, which was published in June of 2002. His co-editors were Dr. A.T. Lin and Prof. K.R. Chu. The 63 articles in this issue, spanning a wide range of topics, attest to the extremely dynamic research and development activities in the field of high power microwave generation by vacuum electronic devices. Three excellent invited review articles are included in this issue. Tim Luce reviewed the current status of electron cyclotron resonance heating (ECRH) and current drive in fusion research reactors. Manfred Thumm and Walter Kasperek discussed some of the components needed for ECRH in their review of the state-of-the-art in passive high power millimeter-wave components. In addition, Monica Blank et al. reviewed the recent development of their high average power W-